Sources of Off-Target Effects of Vagus Nerve Stimulation Using the Helical Clinical Lead in Domestic Pigs

Evan N. Nicolai[1,3], Megan L. Settell[1,3], Bruce E. Knudsen[1,4], Andrea L. McConico[4], Brian A. Gosink[1,2], James K. Trevathan[1], Ian W. Baumgart[1], Erika K. Ross[6], Nicole A. Pelot[5], Warren M. Grill[5], Kenneth J. Gustafson[7,8], Andrew J. Shoffstall[7,8], Justin C. Williams[1,2], Kip A. Ludwig[1,2]

[1] University of Wisconsin-Madison, Department of Biomedical Engineering, Madison, WI, USA
[2] University of Wisconsin-Madison, Department of Neurosurgery, Madison, WI, USA
[3] Mayo Clinic, Mayo Clinic Graduate School of Biomedical Sciences, Rochester, MN, USA
[4] Mayo Clinic, Department of Neurosurgery, Rochester, MN, USA
[5] Duke University, Department of Biomedical Engineering, Durham, NC, USA
[6] Abbott Neuromodulation, Plano, TX, USA
[7] Case Western Reserve University, Department of Biomedical Engineering, Cleveland, OH, USA
[8] Louis Stokes Cleveland VA Medical Center, Cleveland, OH, USA

***Corresponding Last Author**
Kip Ludwig, PhD
Kip.ludwig@wisc.edu
WIMR 2 RM 3548
1111 Highland Ave.
Madison, WI 53705
608-265-3544

Abstract

Cervical vagus nerve stimulation (VNS) with a surgically implanted electrode is a Food and Drug Administration (FDA)-approved treatment for epilepsy and depression. Additionally, VNS is in clinical trials for diverse conditions such as hypertension, heart failure, rheumatoid arthritis, tinnitus, and stroke rehabilitation. Despite the growing use of VNS therapies, clinical data suggest that efficacious stimulation is often limited by side effects such as cough and dyspnea that have stimulation thresholds lower than those for specific therapeutic outcomes. The therapy-limiting side effects are putatively caused by activation of nearby muscles within the neck, either via direct muscle activation or through activation of the nerve fibers innervating those muscles.

Our goal was to determine the thresholds at which various VNS effects occur in the domestic pig—the animal model most similar to humans in terms of vagus nerve size, complexity of fascicular organization, and relative anatomy—using the bipolar helical lead deployed clinically. Intrafascicular electrodes were placed within the vagus nerve to record electroneurographic (ENG) responses, and needle electrodes were placed in the vagal-innervated neck muscles to record electromyographic (EMG) responses. Contraction of the cricoarytenoid muscle occurred at relatively low amplitudes (~0.3 mA), and resulted from activation of motor nerve fibers in the cervical vagus trunk within the electrode cuff which eventually became part of the recurrent laryngeal branch of the vagus. At higher amplitudes (~1.4 mA), contraction of the cricoarytenoid and cricothyroid muscles was generated by current leakage outside the cuff to activate motor nerve fibers running within the nearby superior laryngeal branch of the vagus. Activation of these muscles generated artifacts in the ENG recordings that may be mistaken for more slowly conducting Aδ-, B-, and C-fibers. These data resolve conflicting reports of the stimulation amplitudes required for C-fiber activation in large animal studies (>10 mA) and human studies (<250 μA). After removing these artifacts, ENG signals with post-stimulus latencies consistent with Aδ- and B-fibers occurred in a small subset of animals, and these signals had thresholds similar to those that caused bradycardia. By identifying specific neuroanatomical pathways that cause off-target effects and characterizing the stimulation dose-response curves for on- and off-target effects, these data will help guide interpretation and optimization of clinical VNS.

Introduction

The cervical vagus nerve provides an entry point for modulating both visceral organ function and much of the brain. The human cervical vagus contains a complex mixture of sensory afferents that project to the nucleus tractus solitarius, which projects to diffuse regions of the brain (Altschuler et al., 1989; Kalia & Mesulam, 1980), preganglionic parasympathetic efferents projecting to many viscera (Agostoni et al., 1957; Foley & DuBois, 1937; Hoffman & Schnitzlein, 1961; Mei et al., 1980), and somatic motor efferents projecting to muscles of the neck. Therapeutic vagus nerve stimulation (VNS) with implanted electrodes has grown over recent years for diverse conditions from epilepsy to obesity and several others (De Ferrari et al., 2017; Kimberley et al., 2018; Koopman et al., 2016; Morris et al., 2013; Ng et al., 2016; Tyler et al., 2017; Wheless et al., 2018). Despite remarkable outcomes in some patients across numerous pathologies, side effects are reported in up to 66% of patients, including cough, throat pain, voice alteration, difficulty swallowing, and dyspnea (De Ferrari et al., 2017; Handforth et al., 1998; VNS Study Group, 1995), and are a significant barrier to effective therapy. In an early study of VNS for epilepsy in humans, patients were unable to tolerate stimulation amplitudes higher than 1.3 mA on average using a 500 μs pulse width at 30 Hz (Handforth et al., 1998). Similarly, in a recent clinical trial, the average tolerable amplitude was 1.2 mA using a 300 μs pulse width at 20 Hz and only 12% of patients experienced VNS-evoked heart rate changes 1 year post-implant (De Ferrari et al., 2017). In the present study, we sought to characterize the neuroanatomical pathways responsible for VNS-induced neck muscle contraction putatively associated with therapy-limiting side effects.

We hypothesized that activation of efferent A-type motor nerve fibers within or near the vagus nerve was causing neck muscle contraction in response to VNS, as opposed to direct electrical activation of the muscles. The thresholds for direct activation of denervated muscle fibers are much higher than for activation of large diameter myelinated motor nerve fibers innervating those muscles (Mortimer 1981). Furthermore, the electric field from an electrode source decreases rapidly with distance from the electrode (Plonsey & Barr, 1995). As the vagus itself has multiple somatic branches, we hypothesized that VNS would 1) at lower amplitudes, activate motor fibers in the cervical vagus trunk within the cuff electrodes that eventually bifurcate into the recurrent laryngeal branch of the vagus terminating in the cricoarytenoid muscles, and then 2) at higher amplitudes, activate the motor fibers ‘en passant’ in the nearby superior laryngeal branch of the vagus which terminate in both the cricoarytenoid and cricothyroid muscles (Settell et al., 2019).

To test this hypothesis, anesthetized domestic pigs were acutely stimulated with the bipolar helical lead used for clinical VNS. The domestic pig was chosen due to its anatomical similarities to human (Ding et al., 2012; Hays et al., 2013; Settell et al., 2019). Neck muscle contractions occurred at amplitudes lower than those necessary for producing bradycardia and/or Aδ-, B-, or C-fiber activation. Activation of A-fibers within the cervical vagus trunk that become the recurrent laryngeal branch resulted in contraction of the cricoarytenoid muscle with at long latency, while shorter-latency cricoarytenoid and cricothyroid muscle contractions were caused by the activation of somatic fibers within the nearby superior laryngeal branch by current leakage from the electrodes. Contraction of these muscle groups caused artifacts in the ENG recordings that could easily be mistaken for activation of slower conduction velocity Aδ-, B-, and C-fibers. Following elimination of muscle contractions via neuromuscular blockade or transection of vagus somatic branches, ENG signals consistent with Aδ- and B-fibers were observed in only a small subset of our animals (4 of 13) despite application of stimulation amplitudes (up to 3 mA) over twice average

clinical amplitudes. Likewise, bradycardia was evoked in only 7 of 13 animals and had a higher average threshold (1.6 mA) than clinical averages.

By identifying the neuroanatomical pathways responsible for off-target effects, these data can guide new strategies to avoid these unwanted effects. We also provide the first comprehensive data set in an animal model with similar vagus nerve size and anatomy to humans (Settell et al., 2019) using an unmodified and unscaled helical clinical lead. This comprehensive data set characterizes thresholds for activation and saturation of different fiber types within the cervical vagus, as well as downstream muscle activation and changes in heart rate.

Methods

All animal care and procedures were approved by the Institutional Animal Care and Use Committee of Mayo Clinic. Thirteen pigs were included in the study: seven male pigs, weighing 37.7 ± 2.3 kg (mean ± standard deviation, SD) and six female pigs weighing 38.3 ± 3.9 kg. All procedures described were performed on either the left or right vagus nerve, and only one side per animal.

Anesthesia and Surgical Procedure

All animals were sedated using an intramuscular injection of telazol (6 mg/kg), xylazine (2 mg/kg), and glycopyrrolate (0.006 mg/kg), then intubated and anesthetized using isoflurane (1.5-3% isoflurane in room air). Saline (0.9%) was administered continuously with analgesia (fentanyl, 5 µg/kg bolus i.v., followed by 5 µg/kg/hr in saline drip). Heart rate, respiration, blood pressure, and end-tidal CO_2 were used to assess depth of anesthesia, and isoflurane dosage was adjusted as needed. Animals were euthanized using pentobarbital (100 mg/kg i.v.).

A single incision was made through the skin and superficial fat layers between the mandible and sternal notch using a cautery. Blunt dissection was used to expose the carotid sheath and to separate the vagus nerve from the carotid artery. All attempts were made to leave the vagus nerve undisturbed, while other structures were pulled away from the vagus nerve using vessel loops. The surgical window was kept open throughout the procedure. Pooled liquid in the surgical window was removed periodically, and saline was sprayed evenly through the window to keep all structures moist.

Electrode Types and Surgical Placement

The placement of electrodes in a typical surgical window is shown in Figure 1. The clinical bipolar stimulating electrode (PerreniaFLEX Model 304, 2 mm inner diameter, LivaNova, London, England) was purchased and used without modification. A practicing neurosurgeon assisted in choosing a placement location most similar to human patients. The two contacts were always placed caudal to the superior laryngeal insertion point. The distance between the center of the cranial contact and the superior laryngeal insertion point was 0.49 ± 0.24 cm, and the distance between the center of the caudal contact and the superior laryngeal insertion point was 1.14 ± 0.21 cm.

Bipolar stainless steel needle electrodes were used for measurement of electromyograms (EMG) in the cricothyroid and cricoarytenoid muscles. Custom longitudinal intrafascicular electrodes (LIFEs) were built in-house for measuring electroneurograms (ENG) (based on Lefurge et al.,

1991). Briefly, 300 to 500 µm of insulation was removed at a single location along a 75 µm outer diameter PFA-coated platinum wire (AM-Systems, Sequim, WA) using a thermal wire stripper to create an electrode contact. A suture tie was placed near the location of the electrode contact to assist in tracking the electrode contact during the surgical procedure. A suture needle (Item No. 12050-03, Fine Science Tools, Foster City, CA) was attached to one end of the platinum wire by threading the wire through the needle eyelet and twisting the wire, and an insulated copper extension wire with touchproof connector (441 connector with wire, Plastics1, Roanoke, VA) was soldered to the other end. The needle was used to introduce each LIFE into the vagus nerve, and the needle was removed prior to recordings. Three to five LIFEs were implanted per animal in a staggered cluster (Figure 1a) where the center LIFE was 8.6 ± 1.1 cm caudal to the location of the center of the cranial stimulation electrode contact. Placement of the LIFEs was staggered to prevent exact matching of ENG signal latencies, which could cause the target neural signal to be lost during differential subtraction.

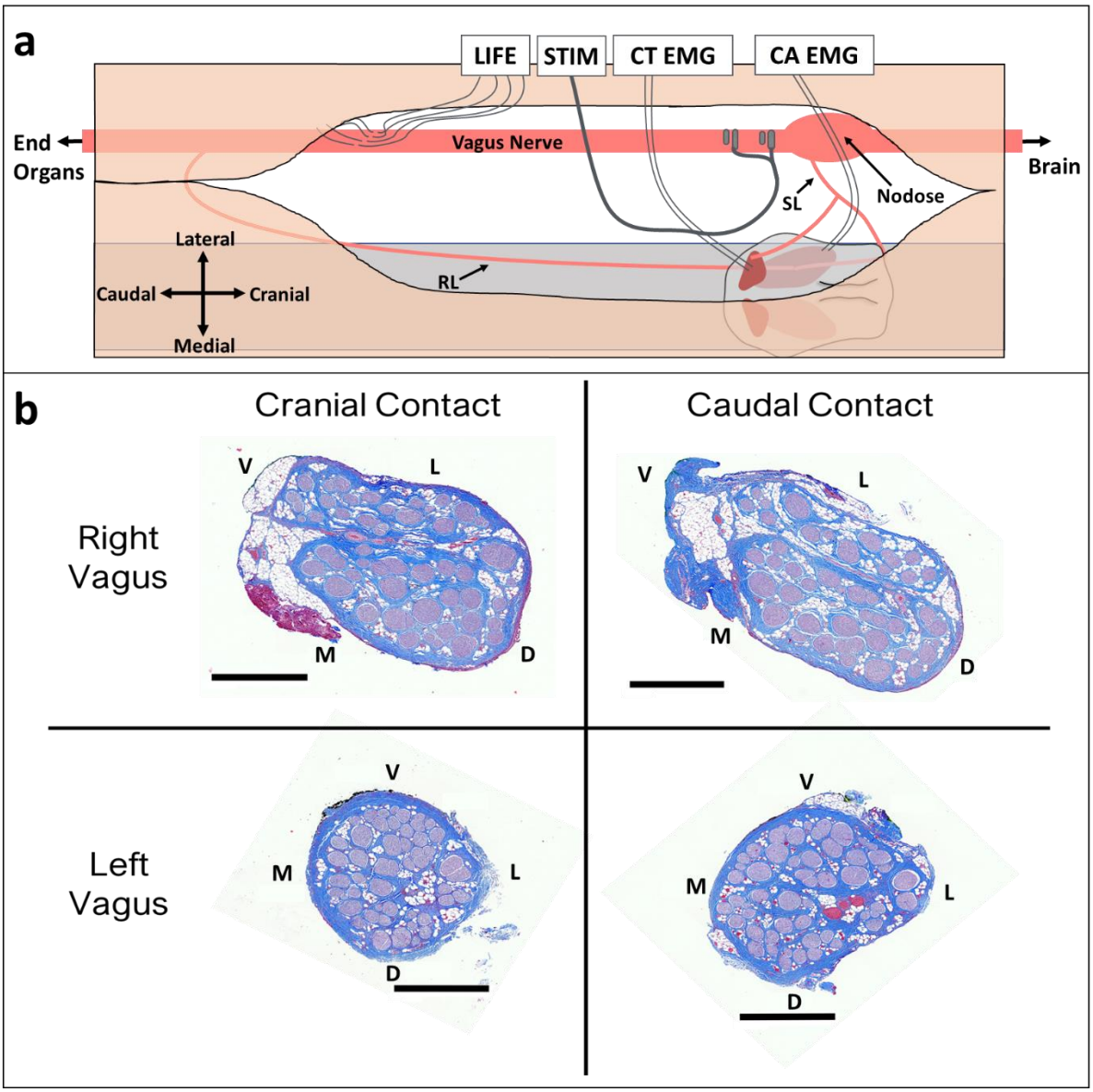

Figure 1: Vagus nerve anatomy and experimental setup. **a)** Diagram (not to scale) of surgical window showing key anatomy and relative electrode locations. Longitudinal intrafascicular electrode (LIFE), stimulation electrode (STIM), cricothyroid muscle (CT), cricoarytenoid muscle (CA), electromyography (EMG), superior laryngeal (SL), recurrent laryngeal (RL). **b)** Representative cross sections from left and right vagus nerves obtained from the location along the vagus nerve where stimulation electrode contacts were placed. Black scale bars are 1 mm. Letters indicate anatomical directions ventral (V), lateral (L), medial (M), and dorsal (D).

Equipment

All LIFE and EMG recordings, as well as stimulations, were performed using a Tucker Davis Technologies system (Alachua, FL; W8, IZ2MH, RZ5D, RZ6, PZ5, and S-Box units). These recordings were collected continuously (24,414 Hz sampling rate, 10,986 Hz anti-aliasing, unity

gain) before, during, and after application of each stimulation pulse. One of the LIFEs was used as the reference electrode for all electrophysiology recordings.

Heart rate and blood pressure were monitored using a pressure catheter (Millar Inc, Houston, TX, Model #SPR-350S) placed into the femoral artery, then digitized and saved using a PowerLab and Bridge Amplifier (ADInstruments, Sydney, Australia).

Experimental Protocol

Bipolar stimulation was delivered at 30 Hz using symmetric biphasic pulses with 200 µs per phase and amplitudes from 50 to 3000 µA evaluated in a random order. Stimulation was typically delivered for 30 s at each amplitude with at least 1 min rest between trials; in some cases, stimulation was delivered for 3 s at each amplitude with at least 10 s rest due to time constraints. Stimulation parameters were chosen to approximate the parameters used in the clinic (De Ferrari et al., 2017; Handforth et al., 1998; VNS Study Group, 1995). In the default bipolar configuration, the more cranial electrode delivered the cathodic phase first. Stimulation with the cathode and anode reversed was also performed in a subset of animals.

Input-output curves were generated from 50 to 3000 µA (including at least 100, 200, 300, 400, 500, 750, 1000, 1500, 2000, 2500, and 3000 µA) in a random order for both cathode cranial and cathode caudal configurations. The full set of amplitudes for cathode cranial and cathode caudal configurations were performed consecutively, one after the other.

To verify the source of EMG and ENG recordings, some stimulation amplitudes – typically 1000, 2000, and 3000 µA – were repeated following a series of perturbations including administration of a neuromuscular blocking agent (vecuronium, 0.1 mg/kg bolus i.v., followed by 3 mg/kg/hr continuous), transection of the recurrent and superior laryngeal vagus nerve branches, and transection of the vagus trunk between the stimulation electrode and LIFEs.

Data Analysis

All signal processing was performed in Matlab R2018b (Mathworks, Natick, MA). ENG and EMG recordings were filtered using a 400 sample median high-pass filter (y=x-medfilt1(x)) and a gaussian low-pass filter (gaussfiltcoef and filtfilt) with corner frequency of 5 kHz. See supplementary information for Matlab code used to process all signals. Stimulation-triggered median traces of evoked LIFE and EMG recordings were calculated for each stimulation amplitude. The activation threshold and latency for each feature were visually identified in the compound action potential and EMG traces (Figure 2). For LIFE recordings, conduction velocities (Aα 70-120 m/s, Aβ 40-70 m/s, Aγ 15-40 m/s, Aδ 5-15 m/s, B 3-14 m/s) (Erlanger & Gasser, 1937; Manzano et al., 2008; Parent & Carpenter, 1996) and measured distances between the electrode delivering cathode phase first and a given LIFE were used to determine latencies for each fiber type. Aα-fibers are not reported here since the short expected latencies (<1 ms) of these fibers were coincident with the stimulation artifact. Aα-fibers are larger diameter than Aβ-fibers, and thus have lower stimulation thresholds; therefore, we made the assumption that measurement of ENGs with post-stimulus latencies consistent with Aβ-fibers was an indication of Aα-fiber activation at a non-measurable lower threshold. Aδ- and B-fibers have overlapping conduction velocities and were therefore treated as one combined neural response (Aδ/B). C-fiber components were not evident in any of our recordings. For most animals, two EMG responses occurred with distinct stimulation thresholds and distinct latencies. The peak of the first major deflection was used to calculate the latency for each response.

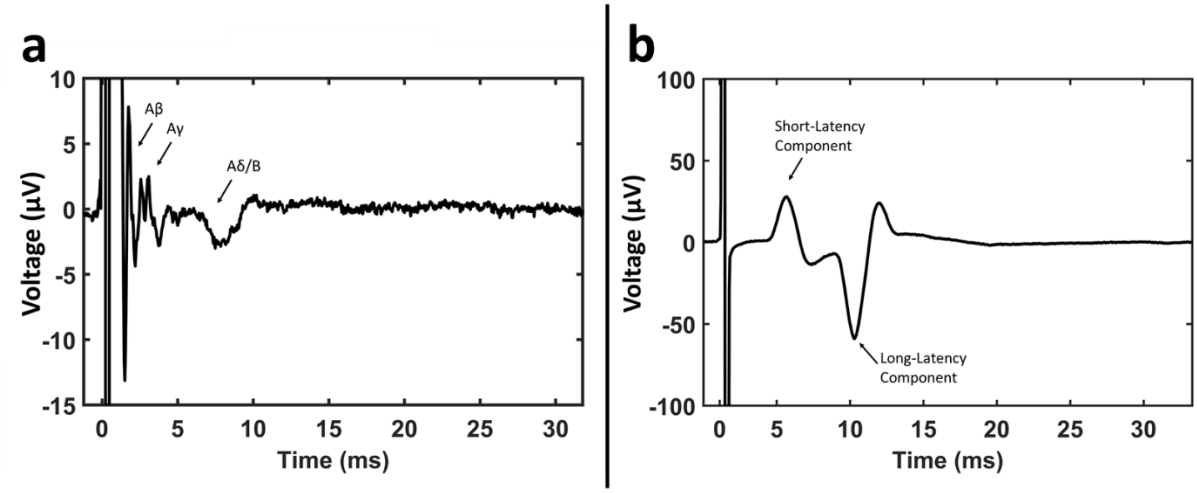

Figure 2: **a)** Example recording from a LIFE showing compound action potential features. **b)** Example EMG recording in the cricothyroid muscle showing short- and long-latency components, with the first major deflection of each component labeled, used to calculate the latencies.

Histological Analysis

Histology dye (Bradley Products, Inc., Davidson Marking System, Bloomington, MN) was placed along the ventral and lateral edge of the vagus nerve to maintain orientation. The nerve was sampled from just cranial to the nodose ganglion to just caudal of the recurrent laryngeal bifurcation, thus including the region of nerve where the stimulating electrode contacts were placed. The samples were placed in 10% neutral buffered formalin for ~24 hr at 4°C. Samples were then placed in a Research and Manufacturing Paraffin Tissue Processor (RMC Ventana Renaissance PTP 1530, Ventana Medical Systems, Oro Valley, AZ) and underwent a series of standard processing steps: 1) dehydration (ethanol, 50-100%), 2) clearing (xylene), and 3) infiltration (paraffin) (Feldman & Wolfe, 2014). Each sample was then embedded in paraffin wax and allowed to set. The block was placed in an ice water bath for approximately one hour to rehydrate the tissue. The block was cut into 5 μm sections using a Leica Biosystems Rotary Microtome (Buffalo Grove, Illinois) and stained using Masson's trichrome. Slides were imaged using a Motic Slide Scanner (Motic North America, Richmond, British Columbia) at 20x.

Results

Neuromuscular Junction Blockade to Determine Pathway Inducing Muscle Contraction

Figure 3 shows stimulation-triggered median ENG and EMG evoked by cervical VNS before and after neuromuscular blockade. As stimulation current was increased (left to right columns), multiple separable signals in both ENG and EMG recordings were observed. Upon neuromuscular blockade, some of the signals were eliminated in the ENG recordings while all the signals were eliminated from the EMG recordings. Neuromuscular blockade either eliminated or greatly

reduced all EMG responses and traces (n = 9); individual traces for each animal can be found in Supplementary Figure 1.

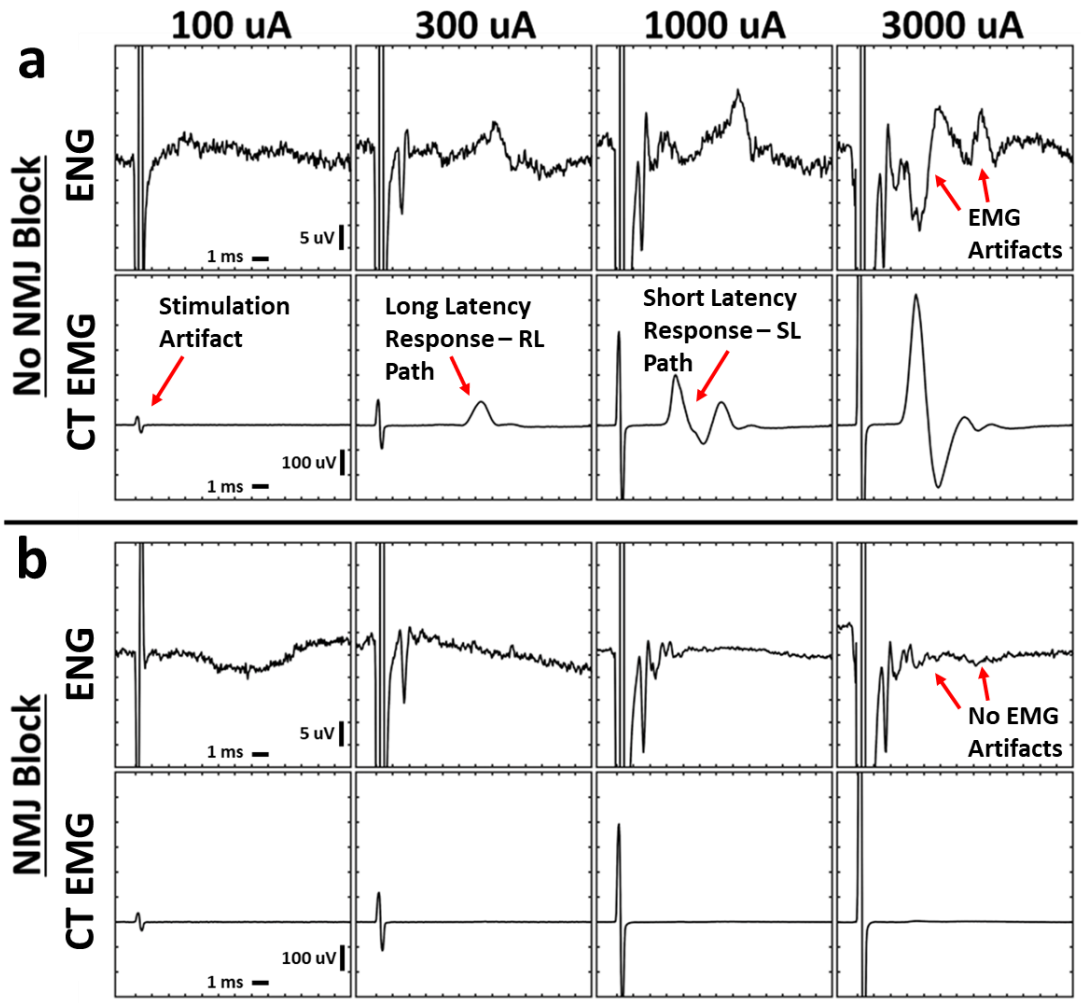

Figure 3: Electromyograms (EMG) exhibited short- and long-latency components at distinct thresholds, and these signals contaminated the electroneurograms (ENG). Neuromuscular blockade with vecuronium eliminated all cricothyroid (CT) and cricoarytenoid (CA, not shown) EMGs and EMG contamination of ENGs. **a)** Simultaneously collected ENG and EMG at multiple stimulation amplitudes (columns) without neuromuscular blockade. **b)** Analogous data in the same animal following neuromuscular blockade. X-axis ticks in all plots are 1 ms. Y-axis ticks are 5 µV in all ENG plots and 100 µV in all EMG plots.

Transection of Somatic Vagus Nerve Branches and the Vagus Trunk to Verify Origins of ENG and EMG

We stimulated before and after transection of each branch to determine whether the branches were required for activation of the cricothyroid and cricoarytenoid muscles by VNS. Additionally,

we transected the vagus trunk between the bipolar electrode contacts and LIFEs to determine whether the recorded ENG signals were indeed compound action potentials evoked by VNS as opposed to additional unanticipated sources of artifact. We first recorded signals with intact nerves, then cut one somatic branch, then cut the other branch, then cut the main trunk (Figure 4a). The order of the branch cuts, SLT and RLT, was sometimes reversed with no observable consequence on outcomes.

Example ENG and EMG traces before and after the transections are shown in Figure 4b. Across all animals (n = 13), transection of the recurrent laryngeal branch (RLT) eliminated the long-latency EMG response, and transection of the superior laryngeal branch (SLT) eliminated the short-latency EMG response (Supplementary Figure 2). Like ENG recordings after neuromuscular blockade, some ENG features were eliminated as a result of each branch transection and were therefore also presumed to be EMG artifact. In all animals, transection of the main vagus trunk eliminated all ENG signals (Supplementary Figure 3). The stimulation artifact remained after all transections.

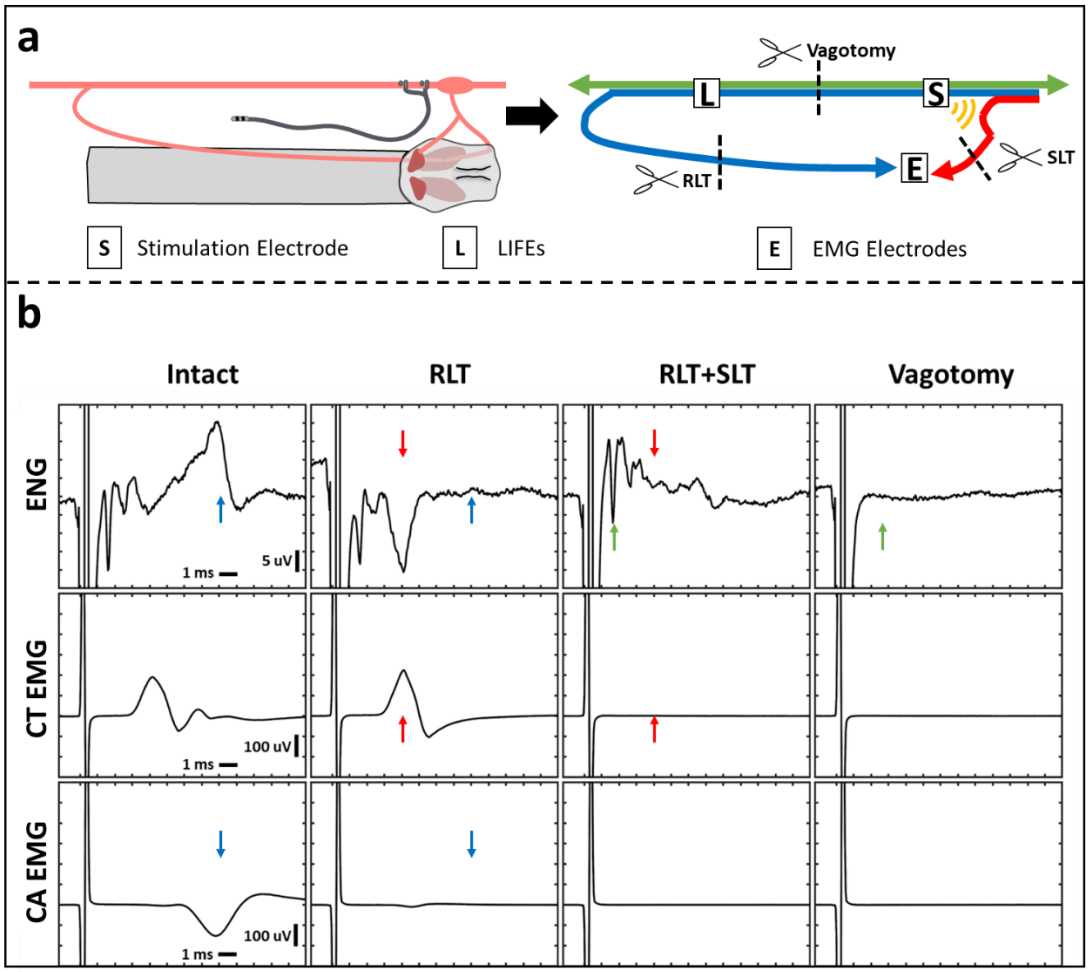

Figure 4: Transection of recurrent laryngeal branch (RLT) and superior laryngeal branch (SLT) eliminated long- and short-latency EMGs, respectively. Transection of the vagus trunk eliminated all ENGs. **a)** Diagram of the transection methods. Left panel shows a diagram of the surgical window. Right panel shows a wiring diagram of nerve fibers with transection locations (scissors). Blue line depicts recurrent laryngeal branch fibers, red line depicts superior laryngeal branch fibers, and green line depicts other vagus nerve fibers. Yellow semi-circles indicate expected current leakage acting on the superior laryngeal branch fibers that do not run within the stimulation electrode. **b)** One channel of ENG (top row) and two channels of EMG (cricothyroid (CT; middle row) and cricoarytenoid (CA; bottom row)) collected simultaneously. Columns represent different time points in order from left to right with an additional transection at each step starting from no transections (Intact, first column). Stimulation parameters for every column are charge-balanced symmetrical biphasic pulses at 3 mA with 200 µs per phase, delivered at 30 Hz for 30 seconds. Paired colored arrows highlight components of the signal that changed before and after each transection.

Stimulation Current Response Curves to Identify ENG and EMG Thresholds for Each Fiber Type

To determine the stimulation threshold for each ENG and EMG response, stimulation-triggered median traces were stacked across stimulation amplitudes to visualize changes in evoked responses (Figure 5a and 5b). For the example in Figure 5, automatic calculation of the rectified area under the curve for each ENG and EMG component within each latency range (i.e., fiber type or EMG component) was used to construct dose-response curves for Aβ-, Aγ-, and Aδ/B-fibers (Figure 5c and 5d), as well as long-component and short-component EMGs (Figure 5e and 5f). Visual inspection of Figure 5a suggests thresholds of ~300, 750, and 2000 μA for activation of Aβ-, Aγ-, and Aδ/B-fibers, respectively, for this example animal. Given temporal mixing of Aβ signals with the larger stimulation artifact and mixing of Aγ signals with the larger Aβ signals, automatic calculation of amplitude and subsequent determination of threshold was challenging in multiple animals. We therefore used visual identification to produce the data found in Supplementary Table 1 by observing figures similar to Figure 5a and 5b for ENGs and EMGs in all animals (Supplementary Figure 4).

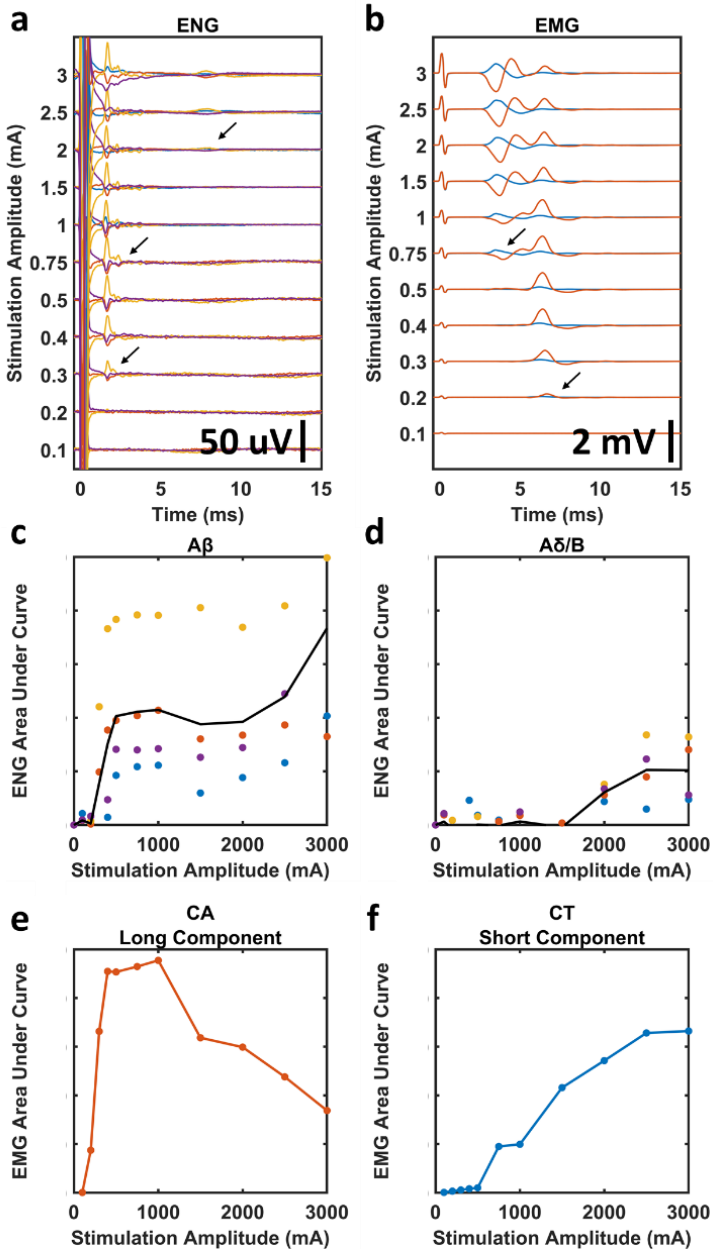

Figure 5: Stimulation dose-response curves and determination of stimulation amplitude threshold for each fiber type. EMG recordings were taken before neuromuscular blockade, ENG recordings were taken in the same animal during neuromuscular blockade. **a)** All stimulation-triggered median ENGs for a representative animal. Arrows indicate visually identified thresholds for each ENG signal; Aβ, Aγ, and Aδ/B from bottom to top. Colored traces represent four different LIFEs. **b)** All stimulation-triggered median EMGs for the same representative animal. Arrows indicate visually identified thresholds for each EMG signal; long-component and short-component from bottom to top. **c-d)** Dose-response curves for Aβ and Aδ/B ENGs calculated using historically available conduction velocities to determine latency ranges. Black line is average of all LIFEs. **e-f)** Dose-response curves for long-component CA and short-component CT EMGs calculated using visually identified latency ranges.

Comparison of Thresholds for On- and Off-Target Effects

The first observable ENG component had a latency consistent with Aβ-fibers and a threshold of 327 ± 215 μA. This is substantially lower than the threshold for ENGs with conduction velocities most consistent with parasympathetic efferents (B-fibers) and/or mechanoreceptor afferents (Aδ-fibers) which was 1875 ± 479 μA. Additionally, Aβ-fiber activation was observed in all animals, while Aδ/B-responses were only observed in 4 of 13 animals even though the same stimulation parameters were applied in every experiment. Consistent with the assertion that measurement of Aβ-fibers was an indication of Aα-fiber activation at a non-measurable lower threshold, the threshold for the long-latency EMG (300 ± 176 μA) was slightly lower – but not significantly different (paired t-test p-value = 0.53) – than the Aβ threshold. The short-latency EMG had a significantly higher threshold (1438 ± 609 μA, paired t-test p-value < 0.01), since the fibers responsible for this response were activated outside of the cuff. Like Aδ/B-responses, HR effects were only observed in a subset of animals – which only partially overlapped with animals that had observable Aδ/B-response – and only seven of thirteen animals had observed HR effects. The threshold for HR changes was 1643 ± 945 μA, which was not significantly different (t-test p-value = 0.83) than the average threshold for Aδ/B-fibers across the cohort. The bradycardia effect had a lower threshold in some animals than the Aδ/B-threshold, and in others a higher threshold (Supplementary Table 1). The thresholds for activation of Aβ-fibers and the long-latency EMG response – were significantly lower (t-test p-value < 0.001) than those thresholds for responses associated with target effects, i.e., activation of Aδ/B-fibers and HR responses (Figure 6).

Comparisons of Vagus Side, Animal Sex, and Stimulus Polarity

Additional analyses were performed to compare ENG and EMG thresholds based on vagus side, animal sex, and stimulus polarity, as well as EMG latencies. Stimulation thresholds for every response except HR were similar between left and right VNS (Figure 6a). However, absolute differences in HR should be interpreted with caution given that isoflurane concentrations were not controlled across animals (see Discussion). No Aδ/B responses were observed in left side VNS experiments (Figure 6a). Unsurprisingly, the long-latency EMG signal had a shorter latency for right side VNS (Figure 6b) given the right recurrent laryngeal branches more cranially – and is thus a shorter path for motor efferents to travel – than the left recurrent laryngeal, including in domestic pigs (Settell et al., 2019). Thresholds and latencies for every response except HR were similar between male and female pigs (Supplemental Figure 5). Stimulation thresholds for Aβ and EMG responses were almost identical between cathode cranial and cathode caudal configurations (Figure 6c); Aγ and Aδ/B responses were not compared since responses following neuromuscular blockade and following nerve branch transections were not collected for most cathode caudal data sets, and thus may contain motor-evoked potential artifacts at the same latencies as Aγ and Aδ/B responses.

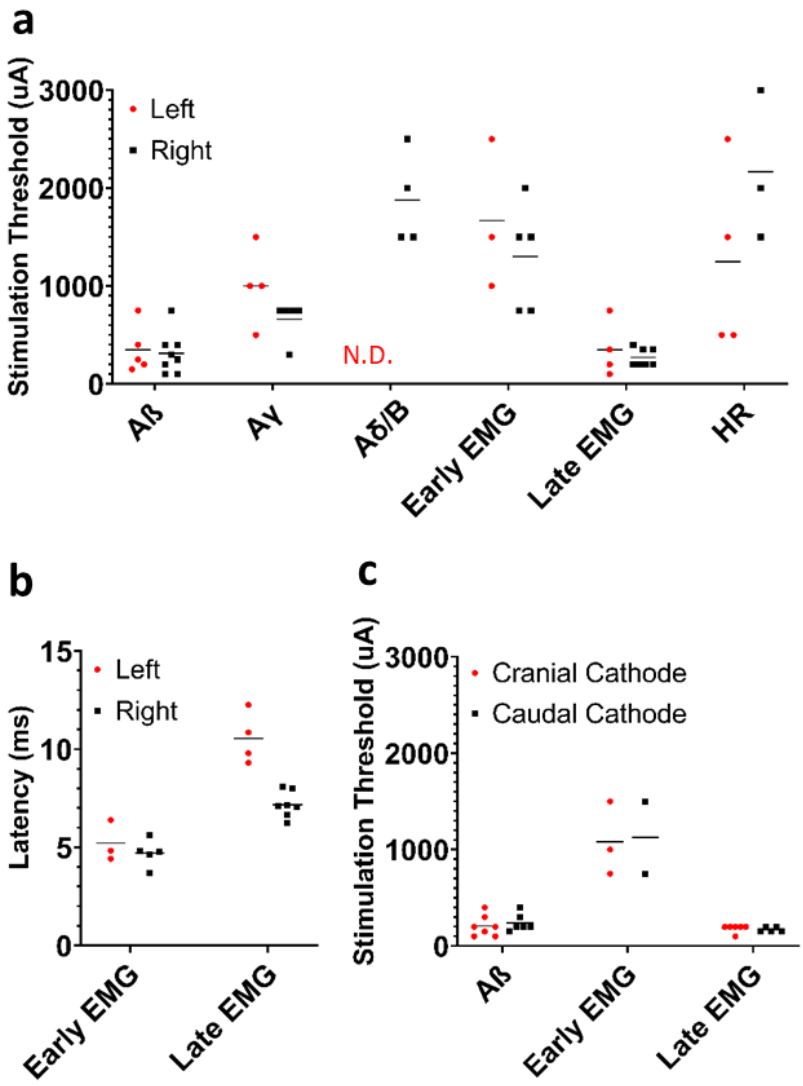

Figure 6: Summary of comparisons between left and right side VNS, as well as cathode and anode configurations. **a)** Thresholds for ENG, EMG, and HR responses comparing left and right vagus nerve experiments. **b)** Post-stimulus latencies for EMG components comparing left and right vagus nerve experiments. **c)** Thresholds for ENG and EMG responses comparing anode and cathode configurations. Note that only paired within-animal data are plotted for panel c.

Discussion

Placing Results in Pig with Clinical Lead in Context of Historic Large Animal and Clinical Studies

Activation of vagal somatic fibers within or near the vagal trunk has long been speculated to be the source of off-target activation of the muscles of the throat/larynx associated with therapy-limiting side effects (Boon et al., 2009; Castoro et al., 2011). Toward that end, several methods were proposed to minimize A-fiber activation and maximize Aδ-, B-fiber or C-fiber activation within cervical vagus trunk including multi-contact electrode arrays to selectively activate certain portions

of the vagal trunk (Aristovich et al., 2019) and different stimulation waveforms to alter the recruitment order, such as anodal block (Accornero et al., 1977), depolarizing prepulses, slowly rising pulses, quasi-trapezoidal pulses (Fang & Mortimer, 1991; M Tosato et al., 2007), and combinations thereof (Vuckovic et al., 2008). Finite element modeling studies also suggest that unintended collateral activation of the nearby superior laryngeal nerve exterior to the vagus nerve at the stimulation site may contribute to off-target effects (Arle et al., 2016). However, prior to the current data, the mechanism of off-target muscle activation had not been carefully verified in a large animal model using an unmodified LivaNova clinical lead.

Somatic fibers within the cuff that eventually branch off into the recurrent laryngeal branch were consistently activated across animals at low amplitudes (0.327 ± 0.215 mA). The threshold for the long latency EMG component via the recurrent laryngeal branch was similar (0.3 ± 0.176 mA). Notably, these stimulation levels are much lower than the average tolerable stimulation amplitudes used clinically (1.2-1.3 mA given similar pulse width) (De Ferrari et al., 2017; Handforth et al., 1998). These data suggest that while the activation of the recurrent laryngeal fibers leads to contraction of neck muscles, these contractions do not manifest as the intolerable side effects observed in patients undergoing VNS.

In contrast, activation of the somatic fibers within the nearby superior laryngeal branch of the vagus due to current leakage from the cuff is more consistent with the tolerable limits to VNS found in human studies. Initial activation of cricoarytenoid and cricothyroid through this pathway was often not observed until 0.75 mA and sometimes did not saturate at our maximally applied amplitude of 3 mA, which is more than double tolerable levels in human studies. It should be noted that the LivaNova helical cuff design has relatively little insulation between the edge of each electrode and the edge of the insulating backer (~1 mm) along the length of the nerve, and consequently may not prevent current leakage as effectively as more extensive epineural cuff designs such as those used in Biocontrol's Cardiofit human studies (De Ferrari et al., 2017).

The goal of this study was to identify the anatomical sources of off-target muscle activation using the most common FDA-approved clinical electrode in a pig animal model best matching the known diameter of the human cervical vagus, at frequencies commonly used to induce changes in sympathetic/parasympathetic tone. This is in contrast to studies using a similar bipolar spiral cuff design in canines (Yoo et al., 2013); in comparison to the human cervical vagus, the canine model is notably smaller diameter, has many fewer fascicles, and has a thicker epineurium that increases the distance from the epineural electrodes to the most superficial fibers. As the epineurium is thinner in pigs and humans than in dogs and thus the most superficial fibers are closer to the electrode, one would anticipate that the thresholds for first observable fiber activation to be lower than in canine studies.

Consistent with this hypothesis, the threshold for activation of large diameter A-fibers in the vagal trunks of pigs was smaller (0.33 ± 0.22 mA, 200 µs pulse width) than the threshold found in a canine study (0.37 ± 0.18 mA, 300 µs pulse width) (Yoo et al., 2013). The prior study also used monophasic instead of biphasic stimulation, which should lower the thresholds for activation by comparison (Merrill 2005). Similarly, the threshold for the EMG component appearing at the lowest stimulation amplitude in pigs was also found to be smaller (0.3 ± 0.18 mA, 200 µs pulse width) than the threshold in canines (0.36 ± 0.17 mA, 300 µs pulse width). It should also be noted in three of the five dogs tested from Yoo et al. 2013, a notable artifact in the electroneurogram recordings was observed with a short post-stimulus latency signal (3 to 5 ms), similar to the response that we demonstrated to be caused by neck muscle contraction via neurotransmission

along the superior laryngeal branch in pigs. As this response had a short post-stimulus latency and was eliminated following the administration of a neuromuscular blocking agent, they hypothesized this component was not related to the activation of the recurrent laryngeal branch. Instead, they proposed this artifact was caused by current spread from the stimulating electrode to a different, unidentified myogenic source (Yoo et al., 2013).

Several important vagus nerve stimulation studies were previously performed in Yorkshire female pigs much larger than those used in our present study (~100 kg) (M Tosato et al., 2007; Marco Tosato et al., 2006). In these studies, homemade tripolar electrodes were used for stimulation which theoretically should increase the rate at which the magnitude of the electric field would decrease with distance from the electrode depending on cathode and anode separation. However, as the focus of the Struijk studies was to explore closed loop paradigms and novel stimulation pulse strategies, data were not collected in such a way that threshold and saturation for A-fiber activation could be directly compared to our study.

Although the latency range used to define B-fibers differed slightly between the aforementioned studies (M Tosato et al., 2007; Marco Tosato et al., 2006; Yoo et al., 2013), both suggested that the threshold for first observing B-fiber activation was near the border of the average tolerated clinical parameters from human studies of 1.2-1.3 mA given 200 µs pulse widths and 20-30 Hz. Similarly, our results indicate that the threshold for activation of Aδ- or B-fibers was 1.88 ± 0.48 mA (200 µs pulse width). In these prior studies, C-fiber activation was observed only at stimulation parameters well beyond levels that are tolerable by human patients (17 ± 7.6 mA with 300 µs pulse width in Yoo et al. 2013; seen only in two cases by Tosato et al. 2006 at ≥6 mA with 600 µs pulse width). C-fiber activation was not observed in our study, unsurprisingly as 3 mA was the maximal stimulation used. We observed extensive concurrent activation of the neck muscles, which tended to cause electrodes to be displaced from tissue, at amplitudes larger than 3 mA. Considering the previous work exploring higher amplitudes – and the lack of clinical relevance in exploring these values due to generation of intolerable side effects – we concluded that there was limited benefit to exploring higher current amplitudes.

The aggregate data across these studies are difficult to reconcile with epineural cuff recordings performed during human VNS surgery (Evans et al., 2004), which observed evoked compound action potential components with a conduction latency consistent with C-fibers. This putative C-fiber component was observed within 10 ms of stimulation, and in two of the patients the “C-fiber” was apparent at the lowest stimulus setting used (0.2 mA, 200 µs pulse width) (Evans et al., 2004). C-fiber responses were reported in all patients, despite the maximal applied amplitude of 3 mA with a pulse width of 200 to 500 µs. As this study was performed opportunistically during human VNS implantation, understandably neither pharmacological muscle block nor transection of the vagus somatic branches was performed to exclude motor-evoked muscle potentials contaminating the ENG recordings. Data from the canine study in which pharmacological neuromuscular junction blockade was performed (Yoo et al., 2013), and our present study sequentially transecting the recurrent laryngeal and superior laryngeal branches, strongly suggest that this response in the human patients was EMG artifact rather than ENG from C-fibers. We specifically show in our current study that long-latency EMG signal via the recurrent laryngeal pathway can create long-latency artifacts in the ENG recordings.

Collectively, these results provide strong evidence that direct activation of C-fibers is unlikely to be the source of VNS therapeutic effects (M Tosato et al., 2007; Marco Tosato et al., 2006; Yoo et al., 2013)(Krahl 2001). Instead, tolerable therapeutic current amplitudes are limited to levels

just at the cusp of activating Aδ-fibers (mechanoreceptor afferents) and B-fibers (pre-ganglionic efferents). Thus, tolerable therapeutic current amplitudes are unlikely to be sufficient to activate the entire population of Aδ-and B-fibers within the cervical vagus. These data would help explain the high variability of therapeutic outcomes for VNS in all indications (De Ferrari et al., 2017; Handforth et al., 1998; Kimberley et al., 2018; Koopman et al., 2016; Tyler et al., 2017). These data are also consistent with a recent rodent study directly comparing optogenetic and electrical activation of the vagus (Rajendran et al., 2019).

Activation of somatic recurrent laryngeal fibers at low thresholds also has important implications for VNS therapeutic mechanisms. Activation of large diameter efferent fibers and the muscles innervated by those fibers at low levels of stimulation presumably would cause indirect activation of sensory pathways below perceptual thresholds (Bruce & White, 2012) which project to the trigeminal sensory nucleus. This produces a possible confound in VNS studies using indirect surrogate measures of nerve engagement such as functional magnetic resonance imaging (fMRI) or somatosensory evoked potentials (SSEPs). In one study exploring VNS using SSEPs in humans, they noted that VNS SSEPs had four signal peaks and that all but the earliest component disappeared after administration of a muscle relaxant (Usami et al., 2013). Indirect activation of this sensory pathway may also have implications for studies of VNS for plasticity such as the hypothesized vagal pathway to facilitate learning that engages nucleus basalis, locus coeruleus, and other brain areas via the nucleus of the solitary tract (Hays et al., 2013).

Implications for Non-Invasive Stimulation of the Cervical Vagus

Our results demonstrate that the large diameter efferent fibers within the cervical vagus that eventually become the recurrent laryngeal branch are activated at much lower thresholds than Aδ-, B-, or C-fibers. Additionally, the motor efferent fibers within the nearby superior laryngeal branch were activated near clinically tolerable levels. It is important to note that the superior laryngeal branch of the vagus can form a ramus of communication with the ascending recurrent laryngeal branch of the vagus nerve underneath or near the thyroid cartilage. This is the location of electrodes for non-invasive VNS, and the distal portions of the superior and recurrent laryngeal branches are much more superficial – closer to the skin of the neck – than the trunk of the cervical vagus nerve.

Activation of the somatic fibers of recurrent and superior laryngeal branches are responsible for activation of the cricoarytenoid and cricothyroid muscles in response to VNS. Therefore, if non-invasive VNS were engaging the pre-ganglionic efferent or sensory afferent fibers of the cervical vagus, presumably one would have to activate these deep muscles of the neck first. However, the off-target effects of invasive VNS including cough, throat pain, voice alteration and dyspnea (De Ferrari et al., 2017; Handforth et al., 1998) are not the off-target effects reported for non-invasive VNS. Non-invasive VNS is known to cause lip curl due to activation of the superficial muscles of the neck (Silberstein et al., 2016), which precludes higher levels of stimulation in clinical practice. In short, even the low threshold motor fibers of the deep vagus are not activated by non-invasive VNS. These data suggest that any therapeutic effect of non-invasive VNS is not through direct activation of the fibers at the cervical vagus, but may be achieving its effects through indirect pathways. For example, sinoatrial baroreceptor afferents have been demonstrated to sometimes also travel through the more superficial recurrent laryngeal branch and return to the cervical vagus via the ramus of communication with the superior laryngeal

branch (Jacobs et al., 1976; Sanders et al., 1987; Strauss et al., 1973). However, a prior study attempting transcutaneous stimulation of the superficial portion of the recurrent laryngeal branch in monkey demonstrated closing of the glottic aperture due to activation of the cricoarytenoid and cricothyroid muscles, but without any cardiac effects (Sanders et al., 1987).

Study Limitations

The isoflurane anesthesia used in our experiments should only impact synaptic transmission (Baumgart et al., 2015; Herring et al., 2009) and would not change the thresholds for direct electrical activation of vagus fibers. Isoflurane is commonly used in vagus and carotid sinus nerve stimulation studies (Georgakopoulos et al., 2009; Thompson et al., 1998), and is not known to impact the stimulation thresholds for motor efferent fibers to elicit muscle contraction. Isoflurane is known to blunt baroreflex mediated cardiac responses (Kotrly et al., 1984; Seagard et al., 1983); however, baroreceptor-induced heart rate changes can still be observed at isoflurane concentrations up to 2.1% (Bagshaw & Cox, 1988). In our study, isoflurane levels were adjusted through the duration of the experiment depending on plane of anesthesia. While all efforts were made to keep the isoflurane concentration as low as possible, isoflurane concentrations at or above 2% were occasionally needed. As cardiac effects were not the primary outcome for these studies, a careful analysis of cardiac response based on isoflourane concentration was not performed. Although robust stimulation-evoked bradycardia was observed at isoflurane concentrations of 2-2.5%, anecdotally these responses were generally smaller than at lower isoflurane concentrations in the same animal. The synaptic blunting caused by isoflurane anesthesia may require activation of a larger number of parasympathetic efferent fibers to the heart or mechanoreceptor afferent fibers to elicit a heart rate response, and therefore change the relationship between the threshold for observing the compound action potential in the neural recordings and the threshold for an associated heart rate response. An additional consideration, due to the sparse sampling nature of the LIFEs for compound action potential measurements, is that in some of our experiments, the LIFEs may have been placed directly inside or adjacent to fascicles containing parasympathetic efferent fibers and may thus cause the apparent threshold for those fibers to be lower than an experiment where the LIFEs were placed in or near fascicles without those fibers. Likewise, these considerations likely contributed to our observation that the apparent threshold for Aδ/B-fibers did not correlate to the apparent threshold for HR effects on an animal by animal basis (Supplementary Table 1).

Moreover, as these experiments were acute, there are several variables that may impact the spatial distribution of applied currents and thus thresholds. The acute surgical trauma often resulted in edema creating fluid at or near the electrode/nerve interface that was tracked visually and removed with surgical gauze when noted. The required cut down and associated surgical pocket displaces tissue in the region nearby the electrode, and it is uncertain if motor nerve fibers other than those of the recurrent laryngeal and superior laryngeal were unintentionally removed from the vicinity of the electrodes. Perhaps most notably, the acute surgical environment does not approximate well the fibrous scar that forms around chronically implanted electrodes, and this would presumably increase the distance of the stimulation electrodes to the nerve trunk.

Finally, the superior laryngeal branch in the pig is located more caudal than human (Settell et al., 2019). In the pig, the superior laryngeal branches within the common surgical window for vagus nerve stimulator implants, whereas in the human the superior laryngeal branches much closer to

the mandible. However, the external branch of the superior laryngeal in the human traverses near the carotid bifurcation and may be affected similarly to the superior laryngeal in pig. Despite these potential limitations, the acute experimental results presented here were consistent with finite element model predictions of human vagus nerve activation (Arle et al., 2016) and stimulation parameters reported tolerable prior to side effects putatively associated with neck muscle contraction in humans (De Ferrari et al., 2017).

Final Thoughts and Next Steps

The FDA-approved human VNS lead by LivaNova consists of two electrodes with active contacts that wrap approximately 270^{o} around the surface of the nerve trunk in a helical cuff, and there is a relatively short distance between the edge of the electrode and the edge of the insulating backer along the length of the nerve. Simple solutions such as increasing the size of the insulating backer or altering the path of the descending external branch of the superior laryngeal during surgery may be sufficient to minimize off-target effects mediated by activation of the superior laryngeal branch in passing.

Avoiding activation of somatic recurrent laryngeal fibers within the cervical vagus nerve in the cuff may be more challenging. One potential solution is a multi-contact array of smaller electrodes (Aristovich et al., 2019) predicated on the idea that there is functional organization of the fibers within the cervical vagus trunk (Settell et al., 2019), termed ‘vagotopy’, that can be leveraged to better isolate vagal fibers associated with specific therapeutic effects. Although there have been demonstrations using multi-contact vagus nerve cuffs in small and large animal models to differentiate between activation of cardiac pathways versus respiratory pathways (Aristovich et al., 2019), it is unknown if there is sufficient functional vagotopy within the cervical vagus nerve to avoid the common therapy-limiting side effect of deep neck muscle activation. Detailed histology of the vagus across animal models and in human subjects has been recently performed (Settell et al., 2019), and additional work to determine exact fiber compositions and locations are warranted, as the specifics may help inform the most simple electrode design in terms of contact size, spacing, overall number and orientation of electrodes that can improve isolation of specific vagal pathways.

The use of tailored stimulation strategies such as anodal block, hyperpolarizing pre-pulses, and guard anodes were proposed to change the ratio of activation between A-, B-, and C-fibers, with some promising results in acute animal models (M Tosato et al., 2007; Marco Tosato et al., 2006; Vuckovic et al., 2008). However, these strategies have not been implemented in clinical settings. This may in part due to the fundamental difficulty in translating new technology into clinical settings. However, these solutions may also be less suitable when scaling to more complex large diameter nerves in the human or large animal model under chronic conditions. In general, as the size of the nerve trunk increases, the distance from the electrode to the fibers of interest increases and spans a larger range, and the thresholds for activation between cathodic or anodic leading biphasic waveforms becomes difficult to distinguish. Consistent with this premise, both in prior canine studies (Yoo et al., 2013) and in the present study, no obvious clinically significant difference was observed in the thresholds for activation when reversing the location of the cathode and anode.

Conclusion

Side effects of VNS present a significant barrier to therapeutic outcomes in the clinic. To better understand the source of these side effects, we stimulated the human-sized cervical vagus of domestic pigs using the same bipolar helical lead used clinically. The cricoarytenoid muscle was activated via motor fibers running within the cuff which eventually become part of the recurrent laryngeal branch at very low thresholds (~0.3 mA). At higher levels of stimulation (~1.4 mA) approaching clinically tolerable limits, current leakage outside of the cuff activated the motor fibers in the nearby superior laryngeal branch, causing contraction of both the cricoarytenoid and cricothyroid muscles. Stimulation at the average tolerable levels derived from clinical studies (~1.3 mA) was often insufficient to activate Aδ- and/or B-fibers and/or evoke bradycardia, and Aδ-/B-fiber activation and bradycardia were not observed in multiple animals despite stimulation amplitudes as high as 3 mA. Our data also suggest that previously reported C-fiber recordings were due to artifacts arising from EMGs elicited by activation of short- and long-latency motor pathways through the superior and recurrent laryngeal branches of the vagus, respectively.

Collectively, these data suggest that the superior laryngeal branch of the vagus nerve may be an anatomical landmark that should be avoided during VNS. Moreover, strategies to avoid the therapy-limiting side effect, such as use of high density epineural electrodes to take better advantage of functional organization within the cervical vagus, should be explored. In addition, mechanisms of VNS that do not depend on direct activation of sensory afferents from the visceral organs should be investigated with increased attention.

Acknowledgements

The authors would like to acknowledge funding from The Defense Advanced Research Projects Agency (DARPA) Biological Technologies Office (BTO) Targeted Neuroplasticity Training Program under the auspices of Doug Weber and Tristan McClure-Begley through the Space and Naval Warfare Systems Command (SPAWAR) Systems Center with (SSC) Pacific grant no. N66001-17-2-4010, NIH SPARC OT2 OD025340, and CTSA Grant Number TL1 TR002380 from the National Center for Advancing Translational Science (NCATS). Its contents are solely the responsibility of the authors and do not necessarily represent the official views of the NIH.

We would like to thank Dr. Jamie J. Van Gompel for guidance on placement of the LivaNova lead in our experiments.

Conflict of Interest Statement

JW and KAL are scientific board members and have stock interests in NeuroOne Medical Inc., a company developing next generation epilepsy monitoring devices. JW also has an equity interest in NeuroNexus technology Inc., a company that supplies electrophysiology equipment and multichannel probes to the neuroscience research community. KAL is also paid member of the scientific advisory board of Cala Health, Blackfynn, Abbott and Battelle. KAL also is a paid consultant for Galvani and Boston Scientific. KAL is a consultant to and co-founder of Neuronoff Inc.

None of these associations are directly relevant to the work presented in this manuscript.

References

Accornero, N., Bini, G., Lenzi, G. L., & Manfredi, M. (1977). Selective Activation of peripheral nerve fibre groups of different diameter by triangular shaped stimulus pulses. *The Journal of Physiology*, *273*(3), 539–560. https://doi.org/10.1113/jphysiol.1977.sp012109

Agostoni, E., Chinnock, J. E., Daly, M. D. B., & Murray, J. G. (1957). Functional and histological studies of the vagus nerve and its branches to the heart, lungs and abdominal viscera in the cat. *The Journal of Physiology*, *135*(1), 182–205. https://doi.org/10.1113/jphysiol.1957.sp005703

Altschuler, S. M., Bao, X., Bieger, D., Hopkins, D. A., & Miselis, R. R. (1989). Viscerotopic representation of the upper alimentary tract in the rat: Sensory ganglia and nuclei of the solitary and spinal trigeminal tracts. *Journal of Comparative Neurology*, *283*(2), 248–268. https://doi.org/10.1002/cne.902830207

Aristovich, K., Donega, M., Fjordbakk, C., Tarotin, I., Chapman, C., Viscasillas, J., Stathopoulou, T.-R., Crawford, A., Chew, D., Perkins, J., & Holder, D. (2019). *Model-based geometrical optimisation and in vivo validation of a spatially selective multielectrode cuff array for vagus nerve neuromodulation*. http://arxiv.org/abs/1903.12459

Arle, J. E., Carlson, K. W., & Mei, L. (2016). Investigation of mechanisms of vagus nerve stimulation for seizure using finite element modeling. *Epilepsy Research*, *126*, 109–118. https://doi.org/10.1016/j.eplepsyres.2016.07.009

Bagshaw, R. J., & Cox, R. H. (1988). Baroreceptor control of central and regional hemodynamics with isoflurane in the dog. *Acta Anaesthesiologica Scandinavica*, *32*(2), 82–92. https://doi.org/10.1111/j.1399-6576.1988.tb02693.x

Baumgart, J. P., Zhou, Z.-Y., Hara, M., Cook, D. C., Hoppa, M. B., Ryan, T. A., & Hemmings, H. C. (2015). Isoflurane inhibits synaptic vesicle exocytosis through reduced Ca 2+ influx, not Ca 2+ -exocytosis coupling. *Proceedings of the National Academy of Sciences*, *112*(38), 11959–11964. https://doi.org/10.1073/pnas.1500525112

Boon, P., Raedt, R., Herdt, V., Wyckhuys, T., & Vonck, K. (2009). Electrical stimulation for the treatment of epilepsy. *Neurotherapeutics*, *6*(2), 218–227. https://doi.org/10.1016/j.nurt.2008.12.003

Bruce, R. M., & White, M. J. (2012). Muscle afferent activation causes ventilatory and cardiovascular responses during concurrent hypercapnia in humans. *Experimental Physiology*, *97*(2), 208–218. https://doi.org/10.1113/expphysiol.2011.061606

Castoro, M. A., Yoo, P. B., Hincapie, J. G., Hamann, J. J., Ruble, S. B., Wolf, P. D., & Grill, W. M. (2011). Excitation properties of the right cervical vagus nerve in adult dogs. *Experimental Neurology*, *227*(1), 62–68. https://doi.org/10.1016/j.expneurol.2010.09.011

De Ferrari, G. M., Stolen, C., Tuinenburg, A. E., Wright, D. J., Brugada, J., Butter, C., Klein, H., Neuzil, P., Botman, C., Castel, M. A., D'Onofrio, A., de Borst, G. J., Solomon, S., Stein, K. M., Schubert, B., Stalsberg, K., Wold, N., Ruble, S., & Zannad, F. (2017). Long-term vagal stimulation for heart failure: Eighteen month results from the NEural Cardiac TherApy foR Heart Failure (NECTAR-HF) trial. *International Journal of Cardiology*, *244*, 229–234. https://doi.org/10.1016/j.ijcard.2017.06.036

Ding, P., Tufano, R. P., & German, R. Z. (2012). Anatomical anomalies of the laryngeal branches of the vagus nerve in pigs (Sus scrofa). *Laboratory Animals*, *46*(4), 338–340. https://doi.org/10.1258/la.2012.012091

Erlanger, J., & Gasser, H. (1937). *Electrical Signs of Nervous Activity*. University of Pennsylvania Press.

Evans, M. S., Verma-Ahuja, S., Naritoku, D. K., & Espinosa, J. A. (2004). Intraoperative human vagus nerve compound action potentials. *Acta Neurologica Scandinavica*, *110*(4), 232–238. https://doi.org/10.1111/j.1600-0404.2004.00309.x

Fang, Z.-P., & Mortimer, J. T. (1991). Selective activation of small motor axons by quasitrapezoidal current pulses. *IEEE Transactions on Biomedical Engineering*, *38*(2), 168–174. https://doi.org/10.1109/10.76383

Feldman, A. T., & Wolfe, D. (2014). *Tissue Processing and Hematoxylin and Eosin Staining* (pp. 31–43). https://doi.org/10.1007/978-1-4939-1050-2_3

Foley, J. O., & DuBois, F. S. (1937). Quantitative studies of the vagus nerve in the cat. I. The ratio of sensory to motor fibers. *The Journal of Comparative Neurology*, *67*(1), 49–67. https://doi.org/10.1002/cne.900670104

Georgakopoulos, D., Wagner, D., Cates, A. W., Irwin, E., & Lovett, E. G. (2009). Effects of electrical stimulation of the carotid sinus baroreflex using the Rheos® device on ventricular-vascular coupling and myocardial efficiency assessed by pressure-volume relations in non-vagotomized anesthetized dogs. *2009 Annual International Conference of the IEEE Engineering in Medicine and Biology Society*, 2025–2029. https://doi.org/10.1109/IEMBS.2009.5334421

Handforth, A., DeGiorgio, C. M., Schachter, S. C., Uthman, B. M., Naritoku, D. K., Tecoma, E. S., Henry, T. R., Collins, S. D., Vaughn, B. V., Gilmartin, R. C., Labar, D. R., Morris, G. L., Salinsky, M. C., Osorio, I., Ristanovic, R. K., Labiner, D. M., Jones, J. C., Murphy, J. V., Ney, G. C., & Wheless, J. W. (1998). Vagus nerve stimulation therapy for partial-onset seizures: A randomized active-control trial. *Neurology*, *51*(1), 48–55. https://doi.org/10.1212/WNL.51.1.48

Hays, S. A., Rennaker, R. L., & Kilgard, M. P. (2013). *Targeting Plasticity with Vagus Nerve Stimulation to Treat Neurological Disease* (pp. 275–299). https://doi.org/10.1016/B978-0-444-63327-9.00010-2

Herring, B. E., Xie, Z., Marks, J., & Fox, A. P. (2009). Isoflurane Inhibits the Neurotransmitter Release Machinery. *Journal of Neurophysiology*, *102*(2), 1265–1273. https://doi.org/10.1152/jn.00252.2009

Hoffman, H. H., & Schnitzlein, H. N. (1961). The numbers of nerve fibers in the vagus nerve of man. *The Anatomical Record*, *139*(3), 429–435. https://doi.org/10.1002/ar.1091390312

Jacobs, J. R., Wetzel, A. B., & Hast, M. H. (1976). Laryngeal Aortic Baroreceptor Pathways and Cardiac Arrhythmia. *Archives of Otolaryngology - Head and Neck Surgery*, *102*(2), 77–79. https://doi.org/10.1001/archotol.1976.00780070055003

Kalia, M., & Mesulam, M. -M. (1980). Brain stem projections of sensory and motor components of the vagus complex in the cat: I. The cervical vagus and nodose ganglion. *Journal of Comparative Neurology*, *193*(2), 435–465. https://doi.org/10.1002/cne.901930210

Kimberley, T. J., Pierce, D., Prudente, C. N., Francisco, G. E., Yozbatiran, N., Smith, P., Tarver, B., Engineer, N. D., Alexander Dickie, D., Kline, D. K., Wigginton, J. G., Cramer, S. C., & Dawson, J. (2018). Vagus Nerve Stimulation Paired With Upper Limb Rehabilitation After Chronic Stroke. *Stroke*, *49*(11), 2789–2792. https://doi.org/10.1161/STROKEAHA.118.022279

Koopman, F. A., Chavan, S. S., Miljko, S., Grazio, S., Sokolovic, S., Schuurman, P. R., Mehta, A. D., Levine, Y. A., Faltys, M., Zitnik, R., Tracey, K. J., & Tak, P. P. (2016). Vagus nerve stimulation inhibits cytokine production and attenuates disease severity in rheumatoid arthritis. *Proceedings of the National Academy of Sciences*, *113*(29), 8284–8289. https://doi.org/10.1073/pnas.1605635113

Kotrly, K. J., Ebert, T. J., Vucins, E., Igler, F. O., Barney, J. A., & Kampine, J. P. (1984). Baroreceptor Reflex Control of Heart Rate during Isoflurane Anesthesia in Humans. *Anesthesiology*, *60*(3), 173–179. https://doi.org/10.1097/00000542-198403000-00001

Lefurge, T., Goodall, E., Horch, K., Stensaas, L., & Schoenberg, A. (1991). Chronically implanted intrafascicular recording electrodes. *Annals of Biomedical Engineering*, *19*(2), 197–207. https://doi.org/10.1007/BF02368469

Manzano, G. M., Giuliano, L. M. P., & Nóbrega, J. A. M. (2008). A brief historical note on the classification of nerve fibers. *Arquivos de Neuro-Psiquiatria*, *66*(1), 117–119. https://doi.org/10.1590/S0004-282X2008000100033

Mei, N., Condamin, M., & Boyer, A. (1980). The composition of the vagus nerve of the cat. *Cell and Tissue Research*, *209*(3). https://doi.org/10.1007/BF00234756

Morris, G. L., Gloss, D., Buchhalter, J., Mack, K. J., Nickels, K., & Harden, C. (2013). Evidence-Based Guideline Update: Vagus Nerve Stimulation for the Treatment of Epilepsy. *Epilepsy Currents*, *13*(6), 297–303. https://doi.org/10.5698/1535-7597-13.6.297

Ng, F. L., Saxena, M., Mahfoud, F., Pathak, A., & Lobo, M. D. (2016). Device-based Therapy for Hypertension. *Current Hypertension Reports*, *18*(8), 61. https://doi.org/10.1007/s11906-016-0670-5

Parent, A., & Carpenter, M. (1996). *Carpenter's Human Neuroanatomy*. Williams & Wilkins.

Plonsey, R., & Barr, R. C. (1995). Electric field stimulation of excitable tissue. *IEEE Transactions on Biomedical Engineering*, *42*(4), 329–336. https://doi.org/10.1109/10.376126

Rajendran, P. S., Challis, R. C., Fowlkes, C. C., Hanna, P., Tompkins, J. D., Jordan, M. C., Hiyari, S., Gabris-Weber, B. A., Greenbaum, A., Chan, K. Y., Deverman, B. E., Münzberg, H., Ardell, J. L., Salama, G., Gradinaru, V., & Shivkumar, K. (2019). Identification of peripheral neural circuits that regulate heart rate using optogenetic and viral vector strategies. *Nature Communications*, *10*(1), 1944. https://doi.org/10.1038/s41467-019-09770-1

Sanders, I., Aviv, J., Racenstein, M. M., Kraus, W. M., & Biller, H. F. (1987). Transcutaneous Electrical Stimulation of the Recurrent Laryngeal Nerve in Monkeys. *Annals of Otology, Rhinology & Laryngology*, *96*(1), 38–42. https://doi.org/10.1177/000348948709600109

Seagard, J. L., Elegbe, E. O., Hopp, F. A., Bosnjak, Z. J., von Colditz, J. H., Kalbfleisch, J. H., & Kampine, J. P. (1983). Effects of Isoflurane on the Baroreceptor Reflex. *Anesthesiology*, *59*(6), 511–520. https://doi.org/10.1097/00000542-198312000-00005

Settell, M. L., Knudsen, B. E., Dingle, A. M., Mcconico, A. L., Nicolai, E. N., Trevathan, J. K., Ross, E. K., Pelot, N. A., Grill, M., Gustafson, K. J., Shoffstall, A. J., & Williams, J. C. (2019). *Functional Vagotopy in the Cervical Vagus Nerve of the Domestic Pig : Implications for Vagus Nerve Stimulation*. 1–28.

Silberstein, S. D., Mechtler, L. L., Kudrow, D. B., Calhoun, A. H., McClure, C., Saper, J. R., Liebler, E. J., Rubenstein Engel, E., & Tepper, S. J. (2016). Non-Invasive Vagus Nerve Stimulation for the AC ute T reatment of Cluster Headache: Findings From the Randomized, Double-Blind, Sham-Controlled ACT1 Study. *Headache: The Journal of Head and Face Pain*, *56*(8), 1317–1332. https://doi.org/10.1111/head.12896

Strauss, S. G., Fukuda, H., & Kirchner, J. A. (1973). Arterial Baroreceptor Fibers in the Recurrent Laryngeal Nerve. *Annals of Otology, Rhinology & Laryngology*, *82*(2), 228–234. https://doi.org/10.1177/000348947308200223

Thompson, G. W., Levett, J. M., Miller, S. M., Hill, M. R. ., Meffert, W. G., Kolata, R. J., Clem, M. F., Murphy, D. A., & Armour, J. A. (1998). Bradycardia Induced by Intravascular Versus Direct Stimulation of the Vagus Nerve. *The Annals of Thoracic Surgery*, *65*(3), 637–642. https://doi.org/10.1016/S0003-4975(97)01351-9

Tosato, M, Yoshida, K., Toft, E., & Struijk, J. J. (2007). Quasi-trapezoidal pulses to selectively block the activation of intrinsic laryngeal muscles during vagal nerve stimulation. *Journal of Neural Engineering*, *4*(3), 205–212. https://doi.org/10.1088/1741-2560/4/3/005

Tosato, Marco, Yoshida, K., Toft, E., Nekrasas, V., & Struijk, J. J. (2006). Closed-loop control of the heart rate by electrical stimulation of the vagus nerve. *Medical & Biological Engineering & Computing*, *44*(3), 161–169. https://doi.org/10.1007/s11517-006-0037-1

Tyler, R., Cacace, A., Stocking, C., Tarver, B., Engineer, N., Martin, J., Deshpande, A., Stecker, N., Pereira, M., Kilgard, M., Burress, C., Pierce, D., Rennaker, R., & Vanneste, S. (2017). Vagus Nerve Stimulation Paired with Tones for the Treatment of Tinnitus: A Prospective Randomized Double-blind Controlled Pilot Study in Humans. *Scientific Reports*, *7*(1), 11960. https://doi.org/10.1038/s41598-017-12178-w

Usami, K., Kawai, K., Sonoo, M., & Saito, N. (2013). Scalp-Recorded Evoked Potentials as a Marker for Afferent Nerve Impulse in Clinical Vagus Nerve Stimulation. *Brain Stimulation*, *6*(4), 615–623. https://doi.org/10.1016/j.brs.2012.09.007

VNS Study Group. (1995). A randomized controlled trial of chronic vagus nerve stimulation for treatment of medically intractable seizures: The Vagus Nerve Stimulation Study Group*. *Neurology*, *45*(2), 224–230. https://doi.org/10.1212/WNL.45.2.224

Vuckovic, A., Tosato, M., & Struijk, J. J. (2008). A comparative study of three techniques for diameter selective fiber activation in the vagal nerve: anodal block, depolarizing prepulses and slowly rising pulses. *Journal of Neural Engineering*, *5*(3), 275–286. https://doi.org/10.1088/1741-2560/5/3/002

Wheless, J. W., Gienapp, A. J., & Ryvlin, P. (2018). Vagus nerve stimulation (VNS) therapy update. *Epilepsy & Behavior*, *88*, 2–10. https://doi.org/10.1016/j.yebeh.2018.06.032

Yoo, P. B., Lubock, N. B., Hincapie, J. G., Ruble, S. B., Hamann, J. J., & Grill, W. M. (2013). High-resolution measurement of electrically-evoked vagus nerve activity in the anesthetized dog. *Journal of Neural Engineering*, *10*(2), 026003. https://doi.org/10.1088/1741-2560/10/2/026003